

1 **The response of the regional longwave radiation balance and climate system**
2 **in Europe to an idealized afforestation experiment**

3
4
5
6
7
8
9
10
11
12
13
14
15
16
17
18
19
20
21
22
23
24
25
26
27
28
29
30
31
32
33
34
35

Marcus Breil^{1,2}, Felix Krawczyk², Joaquim G. Pinto²

¹Institute of Physics and Meteorology, University of Hohenheim, Stuttgart, Germany

²Institute for Meteorology and Climate Research, Karlsruhe Institute of Technology, Karlsruhe, Germany

Correspondence to: Marcus Breil (marcus.breil@uni-hohenheim.de)

36 **Abstract**

37 Afforestation is an important mitigation strategy to climate change due to its carbon sequestration
38 potential. Besides this favorable biogeochemical effect on global CO₂ concentrations, afforestation also
39 affects the regional climate by changing the biogeophysical land surface characteristics. In this study,
40 we investigate the effects of an idealized global CO₂ reduction to pre-industrial conditions by a Europe-
41 wide afforestation experiment on the regional longwave radiation balance, starting in the year 1986
42 from a continent entirely covered with grassland. Results show that the impact of biogeophysical
43 processes on the surface temperatures is much stronger than of biogeochemical processes.
44 Furthermore, biogeophysically induced changes of the surface temperatures, atmospheric
45 temperatures and moisture concentrations are as important for the regional longwave radiation
46 balance as the global CO₂ reduction. While the outgoing longwave radiation is increased in winter, it is
47 reduced in summer. On annual total, a Europe-wide afforestation has a regional warming effect,
48 despite reduced CO₂ concentrations. Thus, even for an idealized reduction of the global CO₂
49 concentrations to pre-industrial levels, the European climate response to afforestation would still be
50 dominated by its biogeophysical effects.

51

52 **1. Introduction**

53 A highly debated strategy to achieve the Paris climate targets is afforestation (Harper et al., 2018; Roe
54 et al., 2019). During their growth period, forests remove CO₂ from the atmosphere and store the
55 carbon in their biomass (Luysaert, et al., 2010; Pan et al., 2011). CO₂ concentrations in the atmosphere
56 are consequently reduced, resulting in a reduction of the downwelling longwave radiation (DLR) and
57 an increase of the outgoing longwave radiation at the top of the atmosphere (OLR). In this way,
58 afforestation actively reduces the greenhouse effect itself.

59 Besides this favorable biogeochemical impact on the global climate system, afforestation affects also
60 the regional climate by changing the biogeophysical characteristics of the land surface (Pielke et al.,
61 2011; Bright et al., 2017). In general, the albedo of forests is lower than of other natural land covers.
62 As a result, more shortwave radiation is absorbed, counteracting the increased OLR (Bala et al, 2007;
63 Bonan, 2008). Thus, the regional climate effect of afforestation depends on the weighting between
64 biogeochemical changes of the longwave radiation balance and biogeophysical changes of the
65 shortwave radiation balance (Claussen et al., 2001; Pielke et al., 2011).

66 Moreover, biogeophysical changes with afforestation have also a direct effect on the longwave
67 radiation balance. By changing land surface characteristics like albedo, surface roughness or leaf area
68 index, surface temperatures are altered (Lee et al., 2011; Duveiller et al., 2018). Since longwave
69 radiation emissions from the surface are, according to the Stefan-Boltzmann law, a function of the
70 surface temperature (T_s), changes in the longwave radiation emissions follow (Vargas Zeppetello et al.,

71 2019). Moreover, changes in the land surface characteristics with afforestation generally lead to an
72 increase of the turbulent heat fluxes (Burakowski et al., 2018; Breil et al., 2020). Atmospheric
73 temperatures (T_a) are consequently increased (Alkama & Cescatti, 2016; Breil et al., 2020), which in
74 turn affect the longwave radiation emitted by the atmosphere. Furthermore, changes in the
75 evapotranspiration rates alter the water vapor concentrations in the atmosphere (Q_a) (Bonan, 2008).
76 Since water vapor is known to be an important greenhouse gas, changes in its concentrations also
77 affect the atmospheric longwave radiation emissions (Claussen et al., 2001; Swann et al., 2010).

78 In spite of their relevance, these complex biogeophysically induced changes in the longwave radiation
79 balance are generally not considered in the ongoing debate on afforestation as a regional mitigation
80 strategy. In general, studies mainly emphasize the effects of the biogeochemically induced CO₂
81 reduction and the biogeophysically induced changes in the albedo (Claussen et al., 2001; Bala et al.,
82 2007). An all-inclusive understanding of the interrelation between afforestation and the longwave
83 radiation balance is thus missing. The arising question whether biogeophysical changes are regionally
84 strengthening or weakening the favorable biogeochemical impact of afforestation on the longwave
85 radiation balance is thus not yet answered. The goal of this study is to disentangle the contribution of
86 both biogeochemical and biogeophysical processes on the emitted longwave radiation over Europe, in
87 a step towards a physically based comprehensive assessment of afforestation as a regional mitigation
88 strategy to climate change.

89 The study is embedded in the Land Use and Climate Across Scales (LUCAS) project (Davin et al., 2020).
90 LUCAS aims to investigate the impact of land use changes on the European climate by performing
91 Regional Climate Model (RCM) simulations. In the first phase of the project, idealized afforestation
92 experiments were performed. In one experiment, the whole European continent was covered by forest
93 (FOREST), in the other experiment the whole continent was covered by grassland (GRASS). By means
94 of these idealized simulations, the maximum possible effect of afforestation on the European climate
95 could be estimated (Davin et al., 2020; Breil et al., 2020). However, only biogeophysical effects of
96 afforestation are considered in these simulations, since the carbon cycle is generally not included in
97 RCMs. Thus, the removal of CO₂ from the atmosphere was not taken into account.

98 In order to close this gap, an additional FOREST simulation which considers the reduced CO₂
99 concentrations with afforestation (CARBON) is analyzed. By comparing the results of CARBON, FOREST
100 and GRASS with the results of an offline radiative transfer model, the respective contributions of
101 biogeochemical and biogeophysical processes to the regional climate system, and particularly to the
102 longwave radiation balance, can be quantified. Section 2 describes the used methodology. The main
103 results are presented (section 3), followed by the discussion (section 4) and conclusions (section 5).

104

105 **2. Methods**

106 2.1. RCM simulations

107 All simulations (GRASS, FOREST, CARBON) are performed with the RCM CCLM-VEG3D (Breil et al., 2021)
108 for the Coordinated Downscaling Experiment – European Domain (EURO-CORDEX; Jacob et al., 2014)
109 on a horizontal resolution of 0.44° (~50 km). The simulations were driven by ERA-Interim reanalyses
110 (Dee et al., 2011) at the lateral boundaries and the lower boundary over sea. The simulation period is
111 1986–2015. A spin-up of 7 years was performed before 1986. For this spin-up, CCLM-VEG3D was again
112 driven with ERA-Interim reanalyses for the period 1979–1985, whereby the same model setup was
113 used as for the period 1986–2015. The simulated conditions in the soil and in the atmosphere at the
114 end of the spin-up period were then used as initial conditions in the long-term simulation.

115 The applied land use datasets are derived from a MODIS-based present-day land cover map (Lawrence
116 and Chase, 2007), in which the land use classes in each grid cell were set to forest (FOREST, CARBON)
117 or grassland (GRASS), respectively, excluding deserts and glaciers (Davin et al., 2020). In CARBON, the
118 resulting reduction in global CO₂ concentrations by an idealized Europe-wide afforestation (see section
119 2.2) is implemented in CCLM-VEG3D, replacing the historic CO₂ concentrations used in FOREST and
120 GRASS.

121

122 2.2. Carbon sequestration by an idealized Europe-wide afforestation

123 In this idealized afforestation experiment, the whole European continent is afforested, starting from a
124 continent entirely covered with grassland. Fig. 1 shows the respective partitioning of the afforested
125 area in boreal and temperate forests. In this experiment, 405 million hectares of Europe are covered
126 with boreal forests, 848 million hectares with temperate forests, thus 1.253 billion hectares in total.
127 On the basis of recent forest inventory data and the results of long-term ecosystem studies, Pan et al.
128 (2011) estimated the amount of carbon sequestered (biomass + soil) in boreal forests to 239 MgC per
129 hectare, and 155 MgC per hectare in temperate forests. This yields a total amount of 228.3 PgC
130 sequestered by a Europe-wide afforestation.

131 The arising global CO₂ concentrations from this idealized afforestation are calculated according to an
132 analytical approach of Goodwin et al. (2007). Assuming a mature forest and steady-state conditions
133 between the atmosphere and the buffering ocean-mixed-layer on a centennial timescale, changes in
134 the atmospheric CO₂ partial pressure P_{CO_2} are calculated as follows:

135

$$136 \Delta P_{CO_2} = \int_{\Sigma C_1}^{\Sigma C_2} \frac{P_{CO_2}}{I_B} d\Sigma C \quad \text{Eq. (1),}$$

137

138 where I_B is the total carbon inventory of the atmosphere plus the total buffered carbon inventory of
139 the ocean. $d\Sigma C$ is the change in the total amount of carbon in the atmosphere-ocean system. Assuming

140 furthermore that changes in I_B are small compared to the total buffered inventory, Eq. (1) can be
141 integrated to

$$142 \quad P_{CO_2} = P_i e^{\frac{\Delta \Sigma C}{I_B}} \quad \text{Eq. (2),}$$

143 where P_i is the initial partial pressure of carbon dioxide at pre-industrial conditions. $\Delta \Sigma C$ is the
144 difference between the total anthropogenic carbon emissions until the year 1986 when our simulation
145 starts (based on Gütschow et al., 2019), and the amount of carbon that would have been removed
146 from the atmosphere by an idealized Europe-wide afforestation. Terrestrial emissions caused by land
147 use changes are not considered, since land emissions are balanced by the terrestrial CO_2 sink of
148 enhanced plant growth and the lengthening of the growing season (Friedlingstein et al., 2020).

149 According to Eq. (2), a resulting global CO_2 concentration of 279 ppm is calculated, constituting an
150 equilibrium on a centennial timescale. Thus, an idealized Europe-wide afforestation, starting from a
151 continent entirely covered with grassland, would have reduced the global CO_2 concentrations at the
152 beginning of our simulation period from 347 ppm in 1986 to pre-industrial levels. This global CO_2
153 concentration is then implemented in the CARBON simulation. Differences in the CO_2 concentrations
154 between a grassland continent and historic CO_2 concentrations are not considered, in order to enable
155 a direct comparison of the CARBON simulation with the GRASS and FOREST runs, and thus, a consistent
156 decomposition of biogeophysical and biogeochemical effects of afforestation. As a consequence, the
157 CO_2 induced global climate feedbacks are not taken into account.

158

159 2.3. BUGSrad

160 Longwave radiation (DLR and OLR) is an implicit function of T_s , T_a , Q_a and the CO_2 concentrations. While
161 the individual contribution of CO_2 on changes in DLR and OLR can be derived from the difference
162 between CARBON and FOREST, such an attribution is not possible for T_s , T_a and Q_a . Thus, DLR and OLR
163 are additionally recalculated with the offline radiative transfer model BUGSrad (Stephens et al., 2001).
164 BUGSrad solves the radiative transfer equation under the assumption of a plane-parallel atmosphere
165 as proposed by Ritter and Geleyn (1992). Thus, BUGSrad is using the same radiative transfer scheme
166 as it is implemented in CCLM-VEG3D, enabling a direct comparison with the RCM results. However,
167 the radiative schemes in CCLM-VEG3D and BUGSrad are not completely identical. BUGSrad is set up
168 with 6 shortwave and 12 longwave bands, whereas CCLM-VEG3D is set up with 3 shortwave and 5
169 longwave bands.

170 The calculations in BUGSrad are based on mean seasonal profiles of T , Q and pressure simulated in
171 CCLM-VEG3D. Only clear-sky situations (daily mean cloud fraction < 20%) are considered, in order to
172 exclude interfering influences of clouds on the longwave radiation balance. Emissions from the lowest
173 atmospheric level correspond to DLR and emission from the uppermost level correspond to OLR. The

174 calculations are performed for eight different European sub-regions, adopted from the PRUDENCE
175 project (Christensen & Christensen, 2007), shown as red rectangles in Fig. 1.

176 The advantage of such an offline model is that numerous simulations can be performed, in which each
177 component affecting DLR and OLR, can be individually varied. In this way, the sensitivity of DLR and
178 OLR to changes in T_s , T_a and Q_a can be quantified. Subsequently, the respective proportion of each
179 component to changes in DLR and OLR can be quantified by means of a Taylor expansion, whereby the
180 derived sensitivities from the offline simulations constitute the partial derivatives of the Taylor
181 expansion (Shine & Sinha, 1991; Huang et al., 2007). Finally, the individual contributions of T_s , T_a and
182 Q_a to the simulated afforestation effects on DLR and OLR with CCLM-VEG3D are derived by multiplying
183 the changes in the temperature and humidity profiles with the partial derivatives of T_s , T_a and Q_a .

184

185 **3. Results**

186 **3.1. CCLM-VEG3 results**

187 **3.1.1. Effects on mean annual surface temperatures**

188 Fig. 2a shows the differences in DLR between CARBON and FOREST over the whole simulation period.
189 Differences between both RCM simulations are only caused by the regional biogeochemical effects in
190 Europe of afforestation. DLR is reduced in CARBON across Europe, as a result of the reduced CO_2
191 concentrations. This reduced DLR leads to slightly reduced yearly mean T_s in CARBON (Fig. 2b).
192 However, the impact of this biogeochemical effect on T_s is negligible in comparison to the
193 biogeophysically induced changes of T_s (Fig. 2c and Fig. 2d). Fig. 2c shows the differences between
194 FOREST and GRASS for the yearly mean T_s in Europe. Differences between these simulations are only
195 caused by biogeophysical changes with afforestation. The magnitude of the differences between
196 FOREST and GRASS is much higher than between CARBON and FOREST, where only biogeochemical
197 effects are considered. For instance, the biogeochemical effects of afforestation (CARBON-FOREST)
198 lead to a reduction of the mean annual T_s of about -0.06 K in Scandinavia and -0.03 K at the Iberian
199 Peninsula, while the biogeophysical effects (FOREST-GRASS) result in a mean warming of 1.06 K in
200 Scandinavia and a mean cooling of -0.77 K at the Iberian Peninsula. The differences between CARBON
201 and GRASS (Fig. 2d), which can be considered as the total effect of afforestation, since both
202 biogeochemical and biogeophysical processes are taken into account, are consequently mainly caused
203 by biogeophysical processes and of the same magnitude as the differences between FOREST and
204 GRASS (1.0 K in Scandinavia and -0.8 K at the Iberian Peninsula). Thus, even with an idealized reduction
205 of the global CO_2 concentrations to pre-industrial levels by a Europe-wide afforestation, the regional
206 climate response to afforestation would be mainly dominated by biogeophysical effects.

207

208 **3.1.2. Effects on the mean seasonal surface temperatures**

209 The mean seasonal differences in T_s between the CARBON and the GRASS simulation are shown in Fig.
210 3. In the winter season (December to February; DJF), warmer T_s is simulated almost all over Europe
211 except of the Iberian Peninsula (IP, Fig. 3a). In contrast to this warmer T_s in winter, T_s is reduced in
212 summer (June to August; JJA) all over Europe with afforestation (Fig. 3b).

213 The warmer T_s in winter is caused by the masking effect of snow on trees (Essery, 2013). In the case of
214 a snow cover, forests are only partially masked by snow due to their large vegetation height, while
215 grasslands are completely covered with snow. As a result, forests absorb more solar radiation than
216 grasslands in winter, and thus, more energy is available to heat up the vegetation surface. On the
217 Iberian Peninsula, snow is generally not occurring in winter and the differences in absorbed solar
218 radiation are consequently not that strong than for the rest of Europe. Since latent heat fluxes of
219 forests are simultaneously increased in IP in winter (Fig. 4a), a larger part of the incoming radiative
220 energy can be released into the atmosphere and surface temperatures are reduced.

221 In summer, forests are able to efficiently transform the radiative energy input at the surface into
222 increased latent heat (Fig. 4b) and sensible heat fluxes, due to their higher surface roughness, higher
223 biomass and deeper root system in comparison to grasslands. Thus, more turbulent energy is removed
224 from the vegetation surface and transported into the atmosphere than for grasslands (Fig. 4c), with
225 the consequence that all over Europe T_s is reduced in summer with afforestation (Fig. 3b; Burakowski
226 et al., 2018; Breil et al., 2020).

227

228 3.1.3. Effects on the longwave radiation balance

229 Fig. 5 shows the differences between the CARBON and the GRASS simulation for DLR (a+c) and OLR
230 (b+d) for the winter season (a+b) and the summer season (c+d). In winter, DLR is enhanced all over
231 Europe by afforestation, except of IP. This extensive increase in DLR is counterintuitive, since one
232 would rather expect a reduction in DLR due to the reduced atmospheric CO_2 concentrations with
233 afforestation. OLR is also increased in winter all over Europe, which is in turn in line with the reduced
234 atmospheric CO_2 concentrations. In summer, a dipole in the DLR differences between CARBON and
235 GRASS is simulated, with a reduced DLR in central and southern Europe and an increased one in
236 Scandinavia (SC). A similar spatial pattern is simulated for OLR in summer with slightly increased
237 (reduced) OLR in northern Europe (southern Europe).

238 In order to be able to explain these spatial longwave radiation patterns, DLR and OLR are additionally
239 simulated with the offline radiative transfer model BUGSrad. By means of a linearization of these
240 BUGSrad simulations, the respective contributions of biogeophysical (changes in the surface
241 temperatures, atmospheric temperatures and atmospheric water vapor concentrations) and
242 biogeochemical (reduced CO_2 concentrations) processes with afforestation on the longwave radiation
243 balance can be decomposed.

244

245 3.2. BUGSrad results

246 3.2.1. Effects on the longwave radiation balance

247 Fig. 6 shows the differences in DLR (a+c) and OLR (b+d) for the winter (a+b) and the summer season
248 (c+d) between CARBON and GRASS simulated with the BUGSrad radiative transfer model. The blue
249 bars show the total differences in DLR or OLR calculated by the offline model. The other colored bars
250 show the respective contributions of CO₂ (pink), Q_a (green), T_a (yellow) and T_s (black) to changes in DLR
251 and OLR between CARBON and GRASS. Thus, the black, yellow and green bars represent the
252 biophysical effects on the longwave radiation balance with afforestation, the pink bars the
253 biogeochemical ones. The grey bar is the residuum, which is attributed to non-linear effects.

254 The simulated differences between CARBON and GRASS with BUGSrad are in good agreement with the
255 results of CCLM-VEG3D (see Fig. 5). The calculated tendencies of afforestation are similar for the
256 different regions and seasons. BUGSrad is also simulating a Europe-wide increase in DLR (except of IP)
257 and OLR in winter in accordance with CCLM-VEG3D (see Fig. 6a, 6b and Fig. 5a, 5b). The radiative dipole
258 in summer with increased DLR and OLR in northern Europe and reduced DLR and OLR in southern
259 Europe is also consistently simulated with both models (see Fig. 6a, 6b and Fig. 5a, 5b). However, the
260 absolute simulated differences between CARBON and GRASS can be different in some regions or
261 seasons. For instance, the reduction in OLR in SC in summer with afforestation is stronger pronounced
262 in BUGSrad (Fig. 6d) than in CCLM-VEG3D (Fig. 5d), which is also the case for the reduction in DLR in
263 winter in IP (see Fig. 6a, 5a). These differences are most likely caused by the different numbers of
264 shortwave and longwave bands in CCLM-VEG3D and BUGSrad.

265 The linearization of the differences in longwave radiation between CARBON and GRASS with BUGSrad
266 reveals that the increased DLR with afforestation in winter is primarily a result of biogeophysical
267 effects, compensating the attenuating effect of reduced CO₂ concentrations (negative pink bars) on
268 DLR (Fig. 6a). In this context, especially T_s has a strong impact on the differences in DLR (positive black
269 bars). Warmer T_s in winter (Fig. 3a) increase the longwave radiation emitted from the surface (except
270 of IP where T_s is reduced). As a result, more longwave radiation can be absorbed by the atmosphere
271 and reemitted as DLR to the surface. This positive feedback on the DLR is amplified by a generally
272 warmer T_a, which is caused by the increased radiative energy input in winter. In addition, Q_a is
273 increased in Europe, because of the higher evapotranspiration rates of forests in comparison to
274 grasslands (Fig. 4a). Both, warmer T_a and higher Q_a have a reinforcing effect on DLR (positive yellow
275 and green bars). Thus, DLR is enhanced in winter with afforestation although the CO₂ concentrations
276 are reduced.

277 The same biogeochemical and biogeophysical changes of the longwave radiation balance lead to an
278 increase in OLR (Fig. 6b). The increased longwave radiation emissions, caused by the increased T_s,

279 provide more radiative energy that can be released into space (positive black bars). Simultaneously,
280 more longwave radiation can escape the atmosphere, due to reduced CO₂ concentrations (positive
281 pink bars). Therefore, biophysical and biochemical processes amplify each other, resulting in increased
282 OLR given afforestation all over Europe.

283 In contrast to the increased T_s in winter, T_s is reduced in summer with afforestation (Fig. 3b). The
284 longwave radiation emitted from the surface is consequently reduced and less radiative energy can be
285 absorbed and reemitted by the atmosphere (negative black bars in Fig. 6c). In combination with the
286 reduced CO₂ concentrations (negative pink bars), DLR is therefore reduced all over Europe, except of
287 SC (Fig. 6c). There, the T_s reduction with afforestation is quite small (Fig. 3b) and the reduction of
288 longwave radiation emitted from the surface is not as clear as for other areas (slightly negative black
289 bar), thus remaining on a comparatively high level. Additionally, evapotranspiration is strongly
290 increased in SC in summer (Fig. 4b), leading to increased Q_a in the lower troposphere (not shown).
291 Since water vapor is an effective greenhouse gas, increased concentrations contribute to an enhanced
292 absorption of the (just slightly reduced) longwave radiation emitted by the surface (clearly positive
293 green bar in SC). In this way, the biogeophysically induced changes of DLR compensate the attenuating
294 effect of reduced CO₂ concentrations on DLR in SC (negative pink bar).

295 Fig. 6d shows that biogeophysical and biogeochemical changes with afforestation have opposing
296 effects on OLR during summer. However, colder T_s reduce the longwave radiation emissions from the
297 surface, and thus the radiative energy that can be released into space (negative black bars). On the
298 other hand, reduced CO₂ concentrations in the atmosphere lead to a reduced absorption of longwave
299 radiation and more radiation that can pass the atmosphere (positive pink bars). Over central Europe
300 (ME), both processes balance each other leading to a net zero effect. In northern Europe (SC, BI),
301 biogeochemical effects are dominating, since changes in T_s and thus, the longwave radiation emissions
302 are especially in SC quite small. This process is stronger pronounced in BUGSrad than in CCLM-VEG3D.
303 Over southern and eastern Europe (MD, EA), the impact of the biogeophysical changes on OLR is
304 dominating. Here, the reduced longwave radiation emissions of the colder surface are amplified by
305 increased Q_a in the mid-troposphere (not shown), counteracting the effect of the reduced CO₂
306 concentrations.

307

308 **3.3. TOA Energy Balance**

309 The decomposition of the BUGSrad simulations showed that biogeophysical effects of afforestation
310 have a strong impact on the longwave radiation balance, which does consequently not only depend
311 on the removal of CO₂ from the atmosphere. In considering both biogeophysical and biogeochemical
312 effects, the question arises, whether afforestation has in general a warming or a cooling effect on the
313 regional climate in Europe. **Since the regional climate conditions in Europe depend decisively both on**

314 the lateral heat transport and on the radiative energy input, the energy balance at the top of the
315 atmosphere (TOA) is analyzed to quantify the impact of the latter. With this aim, the net longwave
316 radiation leaving the earth system is subtracted from the net shortwave radiation input into the
317 system. In this way, biogeophysical changes in the shortwave radiation balance with afforestation by
318 a reduced surface albedo can be related to changes in the longwave radiation balance, which is
319 affected by both biogeophysical and biogeochemical process, as demonstrated above.

320 Changes in the TOA energy balance between CARBON and GRASS are shown for (a) winter, (b) summer
321 and (c) the whole year in Fig. 7. Red areas indicate regions in which afforestation leads to an increased
322 energy input into the regional climate system in Europe, blue areas indicate regions with a reduced
323 energy input. In winter, the TOA energy balance is increased in southern Europe, the Alpine region,
324 eastern Europe and southern Scandinavia (Fig. 7a). In these regions, the increased longwave radiative
325 energy loss by an increased OLR is compensated by an increased shortwave radiation input. In central
326 Europe, the British Isles and northern Scandinavia, the opposite is the case and the TOA energy balance
327 is decreased or close to zero.

328 In summer, the interplay between changes in OLR and changes in the shortwave radiation lead to a
329 decreased TOA energy balance in central and north-eastern Europe and a strongly increased energy
330 balance in southern Europe as well as parts of Scandinavia (Fig. 7b). Across seasons, the TOA energy
331 balance is almost all over Europe increased with afforestation (Fig. 7c). The increased TOA energy
332 balance in Scandinavia is explained by a strong increase in the net shortwave radiation in spring (Fig.
333 8), due to differences in the snow cover. Afforestation is consequently associated with an increased
334 TOA energy balance over Europe.

335

336 **4. Discussion**

337 Prior to the CARBON simulation, a global atmospheric CO₂ concentration of 279 ppm was calculated
338 as a response to a Europe-wide afforestation at the beginning of our simulation period (1986, see
339 section 2.2). At first glance, this substantial reduction of the global CO₂ concentration to pre-industrial
340 levels is astonishing. However, it has to be considered that the applied method is designed for a mature
341 forest, under the assumption of an equilibrium in the atmosphere-ocean system, which will be
342 achieved only on centennial timescales (Goodwin et al., 2007). An inertial short-term adjustment of
343 the CO₂ concentrations is therefore not considered. In addition, the presented study is an idealized
344 and simplified afforestation experiment, starting from a grassland continent. Thus, it is not a realistic
345 afforestation scenario (Bastin et al., 2019) and areas are afforested, in which the environmental
346 conditions are not actually ideal. Changes in the environmental conditions due to climate change are
347 also not considered. Moreover, ongoing fossil fuel emissions are neglected (Jones et al., 2016) and the
348 carbon already stored in grasslands (soil + biomass) is also not taken into account (Jackson et al., 2002).

349 The real carbon sequestration potential of afforestation should consequently be lower and the
350 reduction in global CO₂ concentrations, associated with a more realistic afforestation scenario, should
351 thus be smaller. Hence, this also means that the effect of biogeophysical processes on the longwave
352 radiation balance is likely to be even stronger in comparison to biogeochemical processes. Thus, the
353 regional warming effect of afforestation in Europe is expected to be even more intense in a realistic
354 setup. This experiment should thus be considered as sensitivity study by which the maximum potential
355 effect of afforestation on the longwave radiation balance and the regional climate was estimated.
356 Such a quantification of the direct impacts of biogeophysical and biogeochemical processes on changes
357 in the longwave radiation balance with afforestation is only possible within idealized RCM simulations,
358 since the indirect effects of global climate feedbacks can be specifically excluded. Moreover, the
359 advantage of RCM simulations is that the physical processes related to the interactions between the
360 land surface (soil and vegetation) and the atmosphere are better resolved than in global climate
361 simulations, whereby relevant land-atmosphere feedbacks are simulated more accurately on the
362 regional scale.

363 However, not all effects of afforestation on the European climate can be fully described on the basis
364 of the applied RCM approach. First, CO₂ dynamics are not considered in the CCLM-VEG3D simulations,
365 since no carbon cycle (Liski et al., 2005) is implemented in the modeling framework. Furthermore, all
366 simulations are driven by ERA-Interim reanalysis, which means present-day atmospheric conditions
367 with recent CO₂ concentrations. The feedbacks of reduced CO₂ concentrations and biogeophysical
368 effects on the global climate system, especially on ocean-atmosphere interactions (Davin & de Noblet-
369 Ducoudré 2010; Swann et al., 2012) as well as on snow and sea ice cover (Donohoe et al., 2014), are
370 consequently not considered.

371 These missing global feedbacks are most likely the reason for the small effects on simulated T_s in
372 Europe by an atmospheric CO₂ reduction to pre-industrial levels (Fig. 2b). This small temperature effect
373 is apparently in contradiction to observations, documenting that increasing CO₂ concentrations led to
374 a considerable warming of up to 1.5 K in Europe until the end of our simulation period in comparison
375 to pre-industrial levels (EEA, 2017). However, the results of our simulations are in line with recent
376 studies providing evidence that the temperature effect of changing CO₂ concentrations is not mainly
377 caused by direct changes in the longwave radiation balance, but by changes in the shortwave radiation
378 balance, which are indirectly induced by changes in global CO₂ climate feedbacks, e.g. ice-albedo
379 feedback associated with changes in the snow and ice cover (e.g., Donohoe et al., 2014). Since such
380 feedbacks are not included in our experiment, we have to conclude that the driving boundary
381 conditions of our simulations are too warm.

382 Based on the above, we can assume that an idealized reduction of the global CO₂ concentrations to
383 pre-industrial conditions by a regional afforestation would have a global cooling effect, due to the

384 global climate feedbacks described above. A consideration of such colder global climate conditions in
385 our experiment would of course have certain implications on the biogeophysical processes in our
386 modeling domain. For instance, driving the CARBON simulation with generally colder boundary
387 conditions would enhance snowfall during winter in Europe. The snow masking effect would
388 consequently be increased and more solar radiation would be absorbed than with present-day
389 boundary conditions. As a result, the TOA energy balance would be further enhanced in winter. This
390 process is already known to be the reason for the general warming effect of afforestation in the high
391 latitudes (e.g. Claussen et al., 2001; Bonan, 2008). Furthermore, more snow accumulation in winter
392 would extend the melting phase in spring and increase the differences in absorbed solar radiation
393 between CARBON and GRASS. Since an increased net shortwave radiation in spring (Fig. 8) is already
394 an important factor for the increased TOA energy balance with afforestation particularly in
395 Scandinavia, the total warming would be intensified.

396 In addition, the impact of wind shear on the turbulent heat exchange is getting stronger for colder
397 atmospheric conditions, since buoyancy becomes smaller (e.g. Breil et al., 2021). That means that the
398 impact of the surface roughness on T_s also becomes stronger. Since the surface roughness of forests is
399 higher than of grasslands, the summertime cooling effect of afforestation on T_s (Fig. 3b) would be
400 increased and emitted longwave radiation would be further reduced. Therefore, the consideration of
401 global climate feedbacks in our modeling approach and thus, a forcing with colder boundary
402 conditions, would even intensify the increased TOA energy balance and the warming effect of
403 afforestation in Europe. An idealized reduction of the global CO_2 concentrations to pre-industrial levels
404 by afforestation would consequently not actually cool the regional climate in Europe to pre-industrial
405 conditions, as the regionally increased TOA energy balance would counteract the global effect.

406 However, all derived results are model dependent and are therefore associated with uncertainties. For
407 instance, the study of Davin et al., (2020) showed that the response of different RCMs to afforestation
408 can be quite different for some climatological quantities like evapotranspiration. For T_s , conversely,
409 afforestation effects are very consistent across the models in Europe. In winter, afforestation generally
410 leads to warmer temperatures, due to the snow masking effect of trees (Davin et al., 2020). In summer,
411 increased turbulent heat fluxes into the atmosphere are consistently simulated with afforestation,
412 generally resulting in a reduction of T_s in the models (Breil et al., 2020). Thus, the presented
413 temperature responses are in good agreement with other modeling results. This is also the case for
414 the simulated net shortwave radiation all over the year in Europe (Davin et al., 2020). Since T_s is
415 according to the BUGSrad analysis the most relevant biogeophysical quantity for the net longwave
416 radiation and thus, in combination with the net shortwave radiation, also for the TOA energy balance,
417 this gives us confidence that our model results are robust.

418

419 **5. Conclusions**

420 In this study, the general effects of biogeophysical and biogeochemical processes on the longwave
421 radiation balance and the regional climate conditions in Europe are analyzed within an idealized
422 Europe-wide afforestation RCM experiment, in which the global CO₂ concentrations were reduced to
423 pre-industrial levels at the beginning of our simulation period. The respective contributions of
424 biogeophysical and biogeochemical effects were decomposed by means of additional offline
425 simulations with a radiative transfer model.

426 Results show that the impact of biogeochemical processes with afforestation on surface temperature
427 (T_s) is negligible in comparison to the biogeophysical effects (Fig. 2). Beyond that, biogeophysical
428 processes affect the regional longwave radiation balance, which is generally thought to be positively
429 influenced by afforestation, due to the net removal of CO₂ from the atmosphere. However, our results
430 provide evidence that biogeophysically induced changes of T_s , T_a and Q_a are at least as important for
431 the longwave radiation balance as the atmospheric CO₂ reduction (Fig. 5 and 6). In particular, the
432 changes in T_s have a considerable impact on the magnitude of the **longwave radiation**, in line with
433 Vargas Zeppetello et al. (2019).

434 While results based on coarser resolved global climate studies rather indicate so far that
435 biogeophysical and biogeochemical effects balance each other in Europe (Claussen et al., 2001, Bala
436 et al., 2007), we provide here evidence that afforestation as implemented in our simulations has a total
437 warming effect on the regional climate (Fig. 7). Thus, the increased shortwave radiation input due to
438 the biogeophysical reduction of the surface albedo, is not compensated by increased longwave
439 radiation emissions, associated with reduced CO₂ concentrations. Even with an idealized reduction of
440 the global CO₂ concentrations to pre-industrial levels, the European climate response would still be
441 dominated by biogeophysical processes associated with Europe-wide afforestation. A sole
442 consideration of forests carbon sequestration potential is therefore not enough to assess the suitability
443 of afforestation as mitigation strategy. We conclude that biogeophysical effects always need to be
444 taken into account comprehensively, particularly as they affect the **outgoing longwave radiation**, which
445 is the reason for the generally positive assessment of afforestation as mitigation strategy.

446

447 **Code availability**

448 The code of CCLM-VEG3D is available upon request from the corresponding author. The code of
449 BUGSrad is available on the BUGSrad GitHub repository (<https://github.com/mattchri/BUGSrad>, last
450 access: 16 November 2022).

451

452 **Data availability**

453 The data that support the findings of this study are available upon reasonable request from the
454 corresponding author.

455

456 **Author contribution**

457 MB designed the study and wrote the paper. MB and FK performed the CCLM-VEG3D simulations and
458 FK performed the BUGSrad simulations. FK analyzed the data and prepared the figures. All authors
459 contributed with discussion, interpretation of results and text revisions.

460

461 **Competing interests**

462 The authors declare that they have no conflict of interest.

463

464 **Financial Support**

465 JGP thanks the AXA Research Fund for support.

466

467 **Acknowledgements**

468 All authors thank Peter Knippertz for the fruitful discussions and his scientific input.

469

470

471

472

473

474

475

476

477

478

479

480

481

482

483

484

485

486

487

488 **References**

489 Alkama, R., and Cescatti, A.: Biophysical climate impacts of recent changes in global forest cover.
490 *Science*, 351(6273), 600-604. DOI: [10.1126/science.aac8083](https://doi.org/10.1126/science.aac8083), 2016.

491
492 Bala, G., Caldeira, K., Wickett, M., Phillips, T. J., Lobell, D. B., Delire, C., and Mirin, A.: Combined climate
493 and carbon-cycle effects of large-scale deforestation. *Proceedings of the National Academy of Sciences*,
494 104(16), 6550-6555. <https://doi.org/10.1073/pnas.0608998104>, 2007.

495
496 Bastin, J. F., Finegold, Y., Garcia, C., Mollicone, D., Rezende, M., Routh, D., Zohner, C., and Crowther, T.
497 W.: The global tree restoration potential. *Science*, 365(6448), 76-79. DOI: [10.1126/science.aax0848](https://doi.org/10.1126/science.aax0848),
498 2019.

499
500 Bonan, G. B.: Forests and climate change: forcings, feedbacks, and the climate benefits of forests.
501 *Science*, 320(5882), 1444-1449. DOI: [10.1126/science.1155121](https://doi.org/10.1126/science.1155121), 2008.

502
503 Burakowski, E., Tawfik, A., Ouimette, A., Lepine, L., Novick, K., Ollinger, S., Zarzycki, C., and Bonan, G.:
504 The role of surface roughness, albedo, and Bowen ratio on ecosystem energy balance in the Eastern
505 United States. *Agricultural and Forest Meteorology*, 249, 367-376.
506 <https://doi.org/10.1016/j.agrformet.2017.11.030>, 2018.

507
508 Breil, M., Davin, E. L., and Rechid, D.: What determines the sign of the evapotranspiration response to
509 afforestation in European summer? *Biogeosciences*, 18(4), 1499-1510. [https://doi.org/10.5194/bg-18-](https://doi.org/10.5194/bg-18-1499-2021)
510 [1499-2021](https://doi.org/10.5194/bg-18-1499-2021), 2021.

511
512 Breil, M., Rechid, D., Davin, E. L., de Noblet-Ducoudré, N., Katragkou, E., Cardoso, R. M., Hoffmann, P.,
513 Jach, L.L., Soares, P.M.M., Sofiadis, G., Strada, S., Strandberg, G., Tölle, M.H., and Warrach-Sagi, K.: The
514 opposing effects of reforestation and afforestation on the diurnal temperature cycle at the surface and
515 in the lowest atmospheric model level in the European summer. *Journal of Climate*, 33(21), 9159-9179.
516 <https://doi.org/10.1175/JCLI-D-19-0624.1>, 2020.

517
518 Bright, R. M., Davin, E., O'Halloran, T., Pongratz, J., Zhao, K., and Cescatti, A.: Local temperature
519 response to land cover and management change driven by non-radiative processes. *Nature Climate*
520 *Change*, 7(4), 296-302. <https://doi.org/10.1038/nclimate3250>, 2017.

521

522 Christensen, J. H., and Christensen, O. B.: A summary of the PRUDENCE model projections of changes
523 in European climate by the end of this century. *Climatic change*, 81(1), 7-30.
524 <https://doi.org/10.1007/s10584-006-9210-7>, 2007.

525

526 Claussen, M., Brovkin, V., and Ganopolski, A.: Biogeophysical versus biogeochemical feedbacks of
527 large-scale land cover change. *Geophysical research letters*, 28(6), 1011-1014.
528 <https://doi.org/10.1029/2000GL012471>, 2001.

529

530 Davin, E. L., and de Noblet-Ducoudré, N.: Climatic impact of global-scale deforestation: Radiative
531 versus nonradiative processes. *Journal of Climate*, 23(1), 97-112.
532 <https://doi.org/10.1175/2009JCLI3102.1>, 2010.

533

534 Davin, E. L., Rechid, D., Breil, M., Cardoso, R. M., Coppola, E., Hoffmann, P., Jach, L. L., Katragkou, E.,
535 de Noblet-Ducoudré, N., Radtke, K., Raffa, M., Soares, P. M. M., Sofiadis, G., Strada, S., Strandberg, G.,
536 Tölle, M. H., Warrach-Sagi, K., and Wulfmeyer, V.: Biogeophysical impacts of forestation in Europe: first
537 results from the LUCAS (Land Use and Climate Across Scales) regional climate model intercomparison.
538 *Earth System Dynamics*, 11(1), 183-200. <https://doi.org/10.5194/esd-11-183-2020>, 2020.

539

540 Dee, D. P., Uppala, S. M., Simmons, A. J., Berrisford, P., Poli, P., Kobayashi, S., Andrae, U., Balmaseda,
541 M. A., Balsamo, G., Bauer, P., Bechthold, P., Beljaars, A. C. M., van de Berg, L., Bidlot, J., Bormann, N.,
542 Delsol, C., Dragani, R., Fuentes, M., Geer, A. J., Haimberger, L., Healy, S. B., Hersbach, H., Holm, E. V.,
543 Isaksen, L., Kallberg, P., Köhler, M., Matricardi, M., McNally, A. P., Monge-Sanz, B. M., Morcrette, J.-J.,
544 Park, B.-K., Peubey, C., de Rosnay, P., Tavolato, C., Thepaut, J.-N., and Vitart, F.: The ERA-Interim
545 reanalysis: Configuration and performance of the data assimilation system. *Quarterly Journal of the*
546 *royal meteorological society*, 137(656), 553-597. <https://doi.org/10.1002/qj.828>, 2011.

547

548 Donohoe, A., Armour, K. C., Pendergrass, A. G., and Battisti, D. S.: Shortwave and longwave radiative
549 contributions to global warming under increasing CO₂. *Proceedings of the National Academy of*
550 *Sciences*, 111(47), 16700-16705, 2014.

551

552 Duveiller, G., Hooker, J., and Cescatti, A.: The mark of vegetation change on Earth's surface energy
553 balance. *Nature communications*, 9(1), 1-12. <https://doi.org/10.1038/s41467-017-02810-8>, 2018.

554

555 EEA, C. C.: Impacts and vulnerability in europe 2016—an indicator-based report. Luxembourg:
556 Publications Office of the European Union, 1, 2017.

557
558 Essery, R.: Large-scale simulations of snow albedo masking by forests. *Geophysical Research Letters*,
559 40(20), 5521-5525. <https://doi.org/10.1002/grl.51008>, 2013.
560
561 Friedlingstein, P., O'Sullivan, M., Jones, M. W., Andrew, R. M., Hauck, J., Olsen, A., Peters, G. P., Peters,
562 W., Pongratz, J., Sitch, S., Le Quéré, C., Canadell, J. G., Ciais, P., Jackson, R. B., Alin, S., Aragão, L. E. O.
563 C., Arneeth, A., Arora, V., Bates, N. R., Becker, M., Benoit-Cattin, A., Bittig, H. C., Bopp, L., Bultan, S.,
564 Chandra, N., Chevallier, F., Chini, L. P., Evans, W., Florentie, L., Forster, P. M., Gasser, T., Gehlen, M.,
565 Gilfillan, D., Gkritzalis, T., Gregor, L., Gruber, N., Harris, I., Hartung, K., Haverd, V., Houghton, R. A.,
566 Ilyina, T., Jain, A. K., Joetzjer, E., Kadono, K., Kato, E., Kitidis, V., Korsbakken, J. I., Landschützer, P.,
567 Lefèvre, N., Lenton, A., Lienert, S., Liu, Z., Lombardozi, D., Marland, G., Metzl, N., Munro, D. R., Nabel,
568 J. E. M. S., Nakaoka, S.-I., Niwa, Y., O'Brien, K., Ono, T., Palmer, P. I., Pierrot, D., Poulter, B., Resplandy,
569 L., Robertson, E., Rödenbeck, C., Schwinger, J., Séférian, R., Skjelvan, I., Smith, A. J. P., Sutton, A. J.,
570 Tanhua, T., Tans, P. P., Tian, H., Tilbrook, B., van der Werf, G., Vuichard, N., Walker, A. P., Wanninkhof,
571 R., Watson, A. J., Willis, D., Wiltshire, A. J., Yuan, W., Yue, X., and Zaehle, S.: Global Carbon Budget
572 2020, *Earth Syst. Sci. Data*, 12, 3269–3340, <https://doi.org/10.5194/essd-12-3269-2020>, 2020.
573
574 Goodwin, P., Williams, R. G., Follows, M. J., and Dutkiewicz, S.: Ocean-atmosphere partitioning of
575 anthropogenic carbon dioxide on centennial timescales. *Global Biogeochemical Cycles*, 21(1), GB1014,
576 <https://doi.org/10.1029/2006GB002810>, 2007.
577
578 Gütschow, J., Jeffery, L., Gieseke, R., and Günther, A.: The PRIMAP-hist national historical emissions
579 time series (1850-2017). V. 2.1. GFZ Data Services. <https://doi.org/10.5880/PIK.2019.018>, 2019.
580
581 Harper, A. B., Powell, T., Cox, P. M., House, J., Huntingford, C., Lenton, T. M., Sitch, S., Burke, E.,
582 Chadburn, S. E., Collins, W. J., Comyn-Platt, E., Daioglou, V., Doelman, J. C., Hayman, G., Robertson, E.,
583 van Vuuren, D., Wiltshire, A., Webber, C. P., Bastos, A., Boysen, L., Ciais, P., Devaraju, N., Jain, A. K.,
584 Krause, A., Poulter, B., and Shu, S.: Land-use emissions play a critical role in land-based mitigation for
585 Paris climate targets. *Nature communications*, 9(1), 1-13. <https://doi.org/10.1038/s41467-018-05340->
586 [z](https://doi.org/10.1038/s41467-018-05340-z), 2018.
587
588 Huang, Y., Ramaswamy, V., and Soden, B.: An investigation of the sensitivity of the clear-sky outgoing
589 longwave radiation to atmospheric temperature and water vapor. *Journal of Geophysical Research:*
590 *Atmospheres*, 112, D05104. <https://doi.org/10.1029/2005JD006906>, 2007.
591

592 Jackson, R. B., Banner, J. L., Jobbágy, E. G., Pockman, W. T., and Wall, D. H.: Ecosystem carbon loss with
593 woody plant invasion of grasslands. *Nature*, 418(6898), 623-626.
594 <https://doi.org/10.1038/nature00910>, 2002.

595

596 Jacob, D., Petersen, J., Eggert, B., Alias, A., Christensen, O. B., Bouwer, L. M., Braun, A., Colette, A.,
597 Deque, M., Georgievski, G., Georgopoulou, E., Gobiet, A., Menut, L., Nikulin, G., Haensler, A.,
598 Hempelmann, N., Jones, C., Keuler, K., Kovats, S., Kröner, N., Kotlarski, S., Kriegsmann, A., Martin, E.,
599 van Meijgaard, E., Moseley, C., Pfeifer, S., Preuschmann, S., Radermacher, C., Radtke, K., Rechid, D.,
600 Rounsevell, M., Samuelsson, P., Somot, S., Soussana J.-F., Teichmann, C., Valentini, R., Vautard, R.,
601 Weber, B., and Yiou, P.: EURO-CORDEX: new high-resolution climate change projections for European
602 impact research. *Regional environmental change*, 14(2), 563-578. [https://doi.org/10.1007/s10113-](https://doi.org/10.1007/s10113-013-0499-2)
603 [013-0499-2](https://doi.org/10.1007/s10113-013-0499-2), 2014.

604

605 Jones, C. D., Ciais, P., Davis, S. J., Friedlingstein, P., Gasser, T., Peters, G. P., Rogelj, J., van Vuuren, D. P.,
606 Canadell, J. G., Cowie, A., Jackson, R. B., Jonas, M., Kriegler, E., Littleton, E., Lowe, J. A., Milne, J.,
607 Shrestha, G., Smith, P., Torvanger, A., and Wiltshire, A.: Simulating the Earth system response to
608 negative emissions. *Environmental Research Letters*, 11(9), 095012. [doi:10.1088/1748-](https://doi.org/10.1088/1748-9326/11/9/095012)
609 [9326/11/9/095012](https://doi.org/10.1088/1748-9326/11/9/095012), 2016.

610

611 Lawrence, P. J., and Chase, T. N.: Representing a new MODIS consistent land surface in the Community
612 Land Model (CLM 3.0). *Journal of Geophysical Research: Biogeosciences*, 112, G01023.
613 <https://doi.org/10.1029/2006JG000168>, 2007.

614

615 Lee, X., Goulden, M. L., Hollinger, D. Y., Barr, A., Black, T. A., Bohrer, G., Bracho, R., Drake, B., Goldstein,
616 A., Gu, L., Katul, G., Kolb, T., Law, B. E., Margolis, H., Meyers, T., Monson, R., Munger, W., Oren, R., Tha
617 Paw U, K., Richardson, A. D., Schmid, H.-P., Staebler, R., Wofsy, S., and Zhao, L.: Observed increase in
618 local cooling effect of deforestation at higher latitudes. *Nature*, 479(7373), 384-387.
619 <https://doi.org/10.1038/nature10588>, 2011.

620

621 Liski, J., Palosuo, T., Peltoniemi, M., and Sievänen, R.: Carbon and decomposition model Yasso for
622 forest soils. *Ecological modelling*, 189(1-2), 168-182.
623 <https://doi.org/10.1016/j.ecolmodel.2005.03.005>, 2005.

624

625 Luysaert, S., Ciais, P., Piao, S. L., Schulze, E. D., Jung, M., Zaehle, S., Schelhaas, M. J., Reichstein, M.,
626 Churkina, G., Papale, D., Abril, G., Beer, C., Grace, J., Loustau, D., Matteucci, G., Magnani, F., Nabuurs,

627 G. J., Verbeeck, H., Sulkava, M., van der Werf, G. R., Janssens, I. A., and members of the CARBOEUROPE-
628 IP SYNTHESIS TEAM: The European carbon balance. Part 3: forests. *Global Change Biology*, 16(5), 1429-
629 1450. <https://doi.org/10.1111/j.1365-2486.2009.02056.x>, 2010.

630

631 Pan, Y., Birdsey, R. A., Fang, J., Houghton, R., Kauppi, P. E., Kurz, W. A., .Phillips, O. L., Shvidenko, A.,
632 Lewis, S. L., Canadell, J. G., Ciais, P., Jackson, R. B., Pacala, S. W., McGuire, A. D., Paio, S., Rautiainen,
633 A., Sitch, S., and Hayes, D.: A large and persistent carbon sink in the world's forests. *Science*, 333(6045),
634 988-993. [DOI: 10.1126/science.1201609](https://doi.org/10.1126/science.1201609), 2011.

635

636 Pielke Sr, R. A., Pitman, A., Niyogi, D., Mahmood, R., McAlpine, C., Hossain, F., Goldewijk, K. K., Nair,
637 U., Betts, R., Fall, S., Reichstein, M., Kabat, P., and de Noblet, N.: Land use/land cover changes and
638 climate: modeling analysis and observational evidence. *Wiley Interdisciplinary Reviews: Climate*
639 *Change*, 2(6), 828-850. [doi: 10.1002/wcc.144](https://doi.org/10.1002/wcc.144), 2011.

640

641 Ritter, B., and Geleyn, J. F.: A comprehensive radiation scheme for numerical weather prediction
642 models with potential applications in climate simulations. *Monthly weather review*, 120(2), 303-325.
643 [https://doi.org/10.1175/1520-0493\(1992\)120<0303:ACRSFN>2.0.CO;2](https://doi.org/10.1175/1520-0493(1992)120<0303:ACRSFN>2.0.CO;2), 1992.

644

645 Roe, S., Streck, C., Obersteiner, M., Frank, S., Griscom, B., Drouet, L., Fricko, O., Gusti, M., Harris, N.,
646 Hasegawa, T., Hausfather, Z., Havlik, P., House, J., Nabuurs, G.-J., Popp, A., Sanz Sanchez, M. J.,
647 Sanderman, J., Smit, P., Stehfest, E., and Lawrence, D.: Contribution of the land sector to a 1.5 C world.
648 *Nature Climate Change*, 9(11), 817-828. <https://doi.org/10.1038/s41558-019-0591-9>, 2019.

649

650 Shine, K. P., and Sinha, A.: Sensitivity of the Earth's climate to height-dependent changes in the water
651 vapour mixing ratio. *Nature*, 354(6352), 382-384. <https://doi.org/10.1038/354382a0>, 1991.

652

653 Stephens, G. L., Gabriel, P. M., and Partain, P. T.: Parameterization of atmospheric radiative transfer.
654 Part I: Validity of simple models. *Journal of the atmospheric sciences*, 58(22), 3391-3409.
655 [https://doi.org/10.1175/1520-0469\(2001\)058<3391:POARTP>2.0.CO;2](https://doi.org/10.1175/1520-0469(2001)058<3391:POARTP>2.0.CO;2), 2001.

656

657 Swann, A. L., Fung, I. Y., Levis, S., Bonan, G. B., and Doney, S. C.: Changes in Arctic vegetation amplify
658 high-latitude warming through the greenhouse effect. *Proceedings of the National Academy of*
659 *Sciences*, 107(4), 1295-1300. <https://doi.org/10.1073/pnas.0913846107>, 2010.

660

661 Swann, A. L., Fung, I. Y., and Chiang, J. C.: Mid-latitude afforestation shifts general circulation and
662 tropical precipitation. *Proceedings of the National Academy of Sciences*, 109(3), 712-716.
663 <https://doi.org/10.1073/pnas.1116706108>, 2012.

664

665 Vargas Zeppetello, L. R., Donohoe, A., and Battisti, D. S.: Does surface temperature respond to or
666 determine downwelling longwave radiation? *Geophysical Research Letters*, 46(5), 2781-2789.
667 <https://doi.org/10.1029/2019GL082220>, 2019.

668

669

670

671

672

673

674

675

676

677

678

679

680

681

682

683

684

685

686

687

688

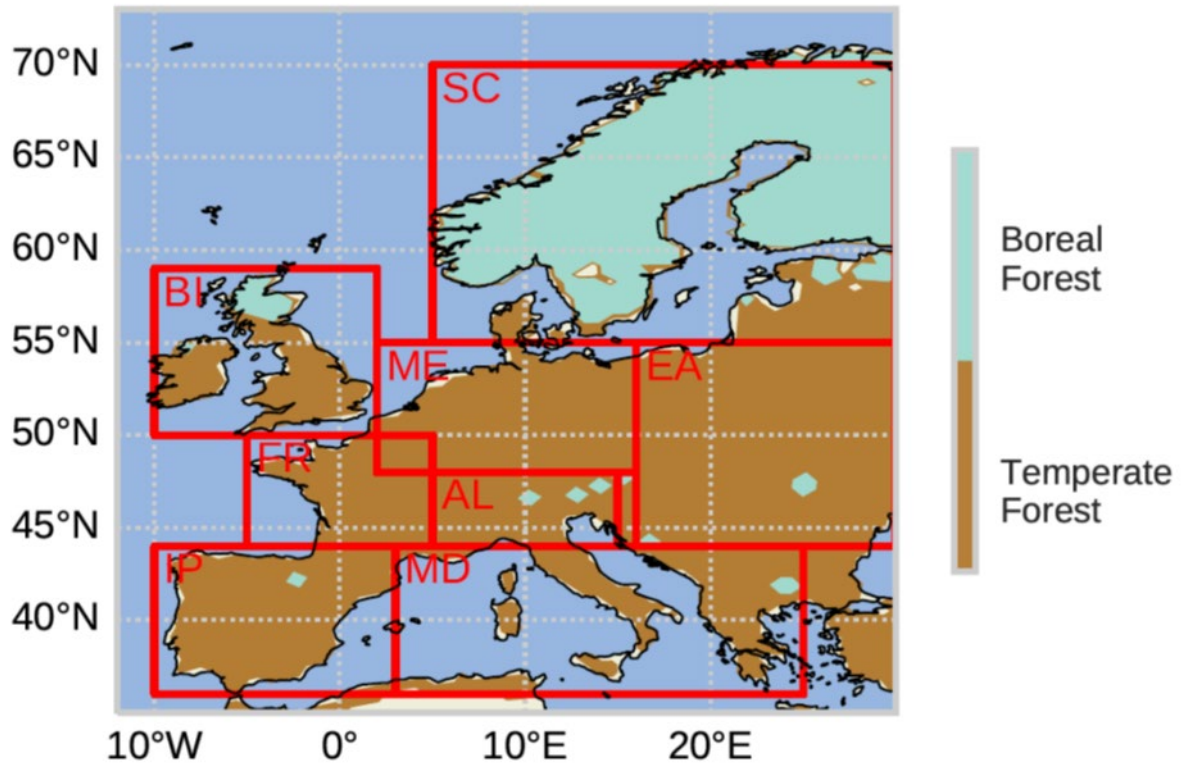
689

690

691

692

693

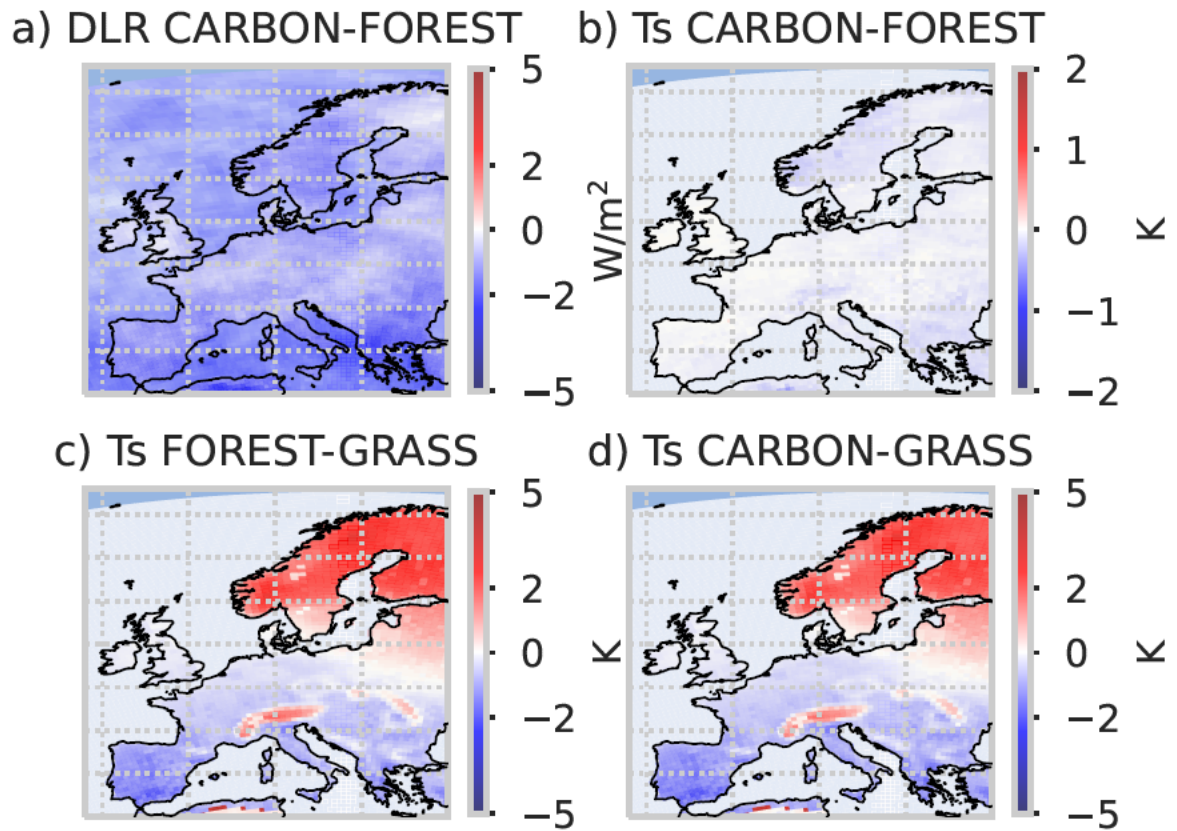


694

695 Figure 1: Spatial distribution of boreal and temperate forests in the CCLM-VEG3D FOREST and CARBON
 696 simulations.

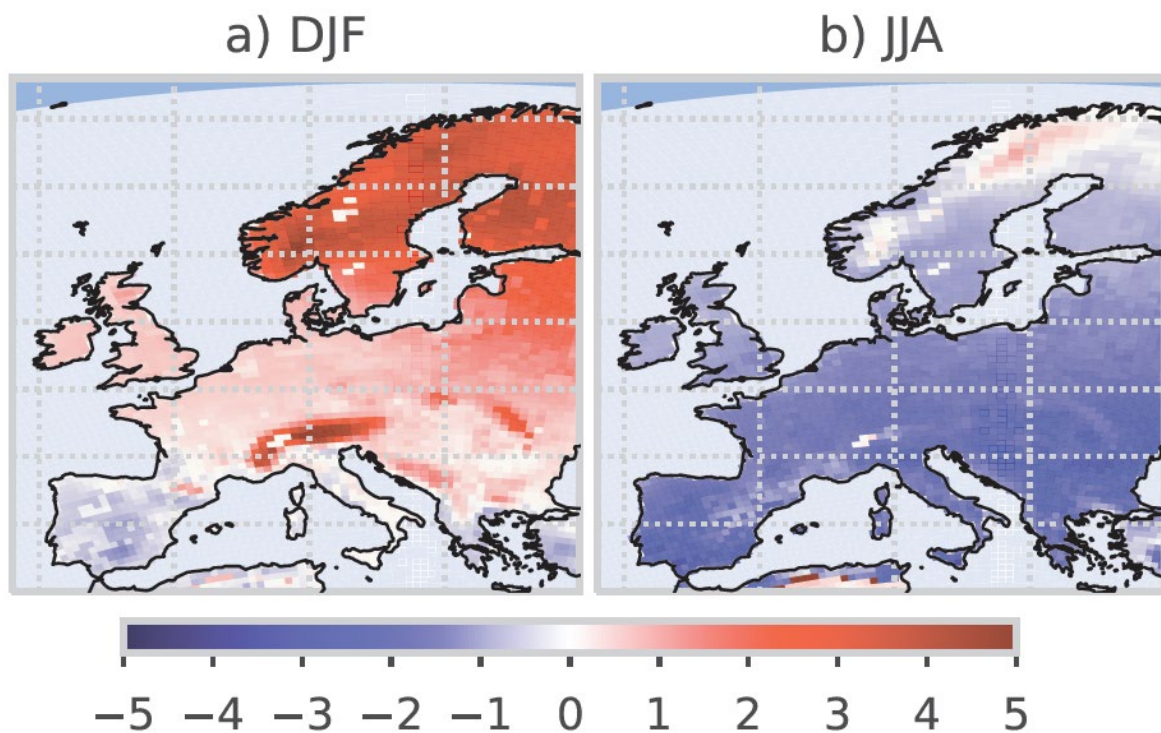
697

698



699
 700 **Figure 2: Yearly mean differences in (a) DLR between CARBON and FOREST, (b) T_s between CARBON**
 701 **and FOREST, (c) T_s between FOREST and GRASS, and (d) T_s between CARBON and GRASS for the period**
 702 **1986-2015.**

703
 704
 705
 706
 707
 708
 709
 710



711

712

713 Figure 3: Mean differences in T_s in [K] between CARBON and GRASS for the period 1986-2015, for the

714 (a) winter season and the (b) summer season.

715

716

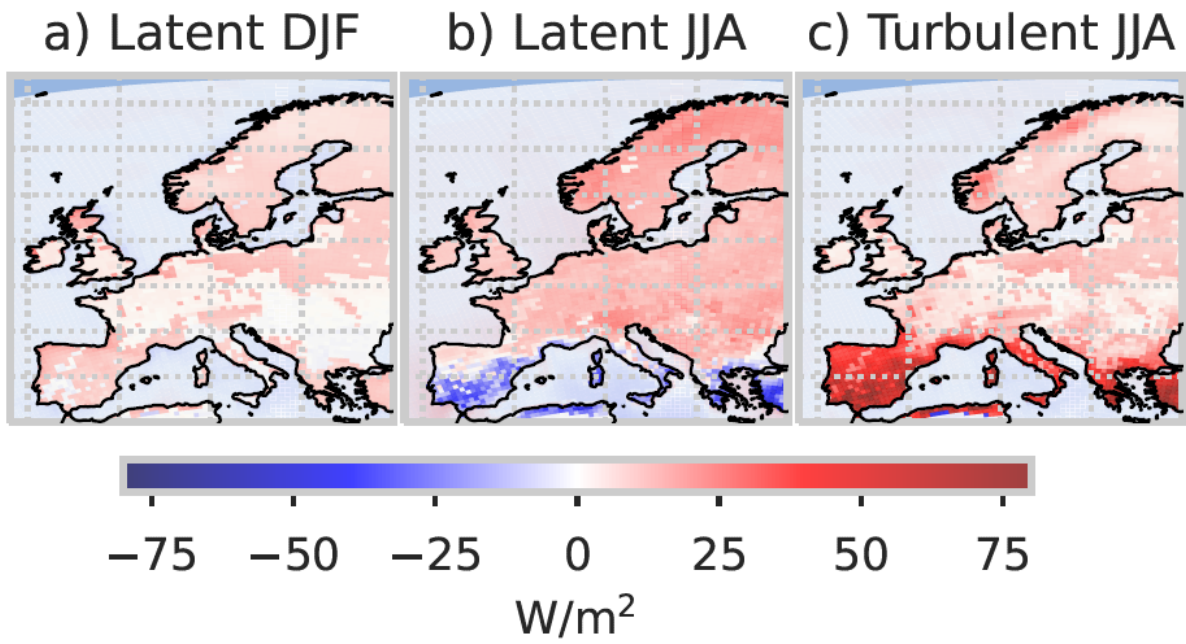
717

718

719

720

721



722

723

724 Figure 4: Mean differences between CARBON and GRASS for the latent heat fluxes in (a) winter and

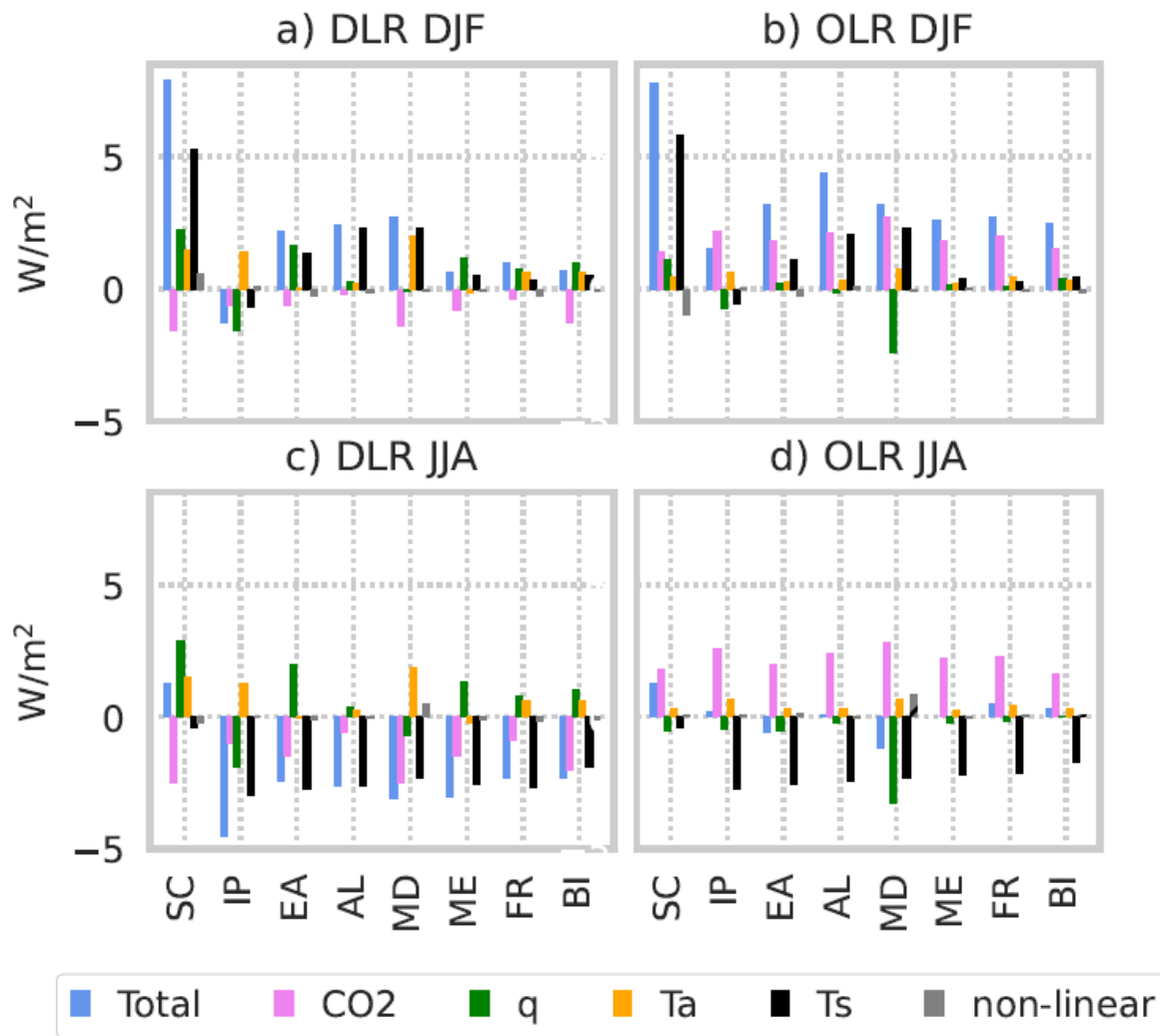
725 (b) summer for the period 1986-2015. The differences in the sum of all turbulent heat fluxes (latent +

726 sensible) in summer is shown in (c).

727

728

729



730

731 **Figure 5:** Differences in DLR (a+c) and OLR (b+d) for the winter (a+b) and the summer season (c+d)
 732 between CARBON and GRASS simulated with BUGSrad. Blue bars show total differences in DLR/OLR.
 733 The other bars show the respective contributions of CO₂ (pink), Q_a (green), T_a (yellow) and T_s (black) to
 734 changes in DLR/OLR. Black, yellow and green bars represent biogeophysical effects on the longwave
 735 radiation balance with afforestation, pink bars biogeochemical effects. The grey bar is the residuum,
 736 which is attributed to non-linear effects.

737

738

739

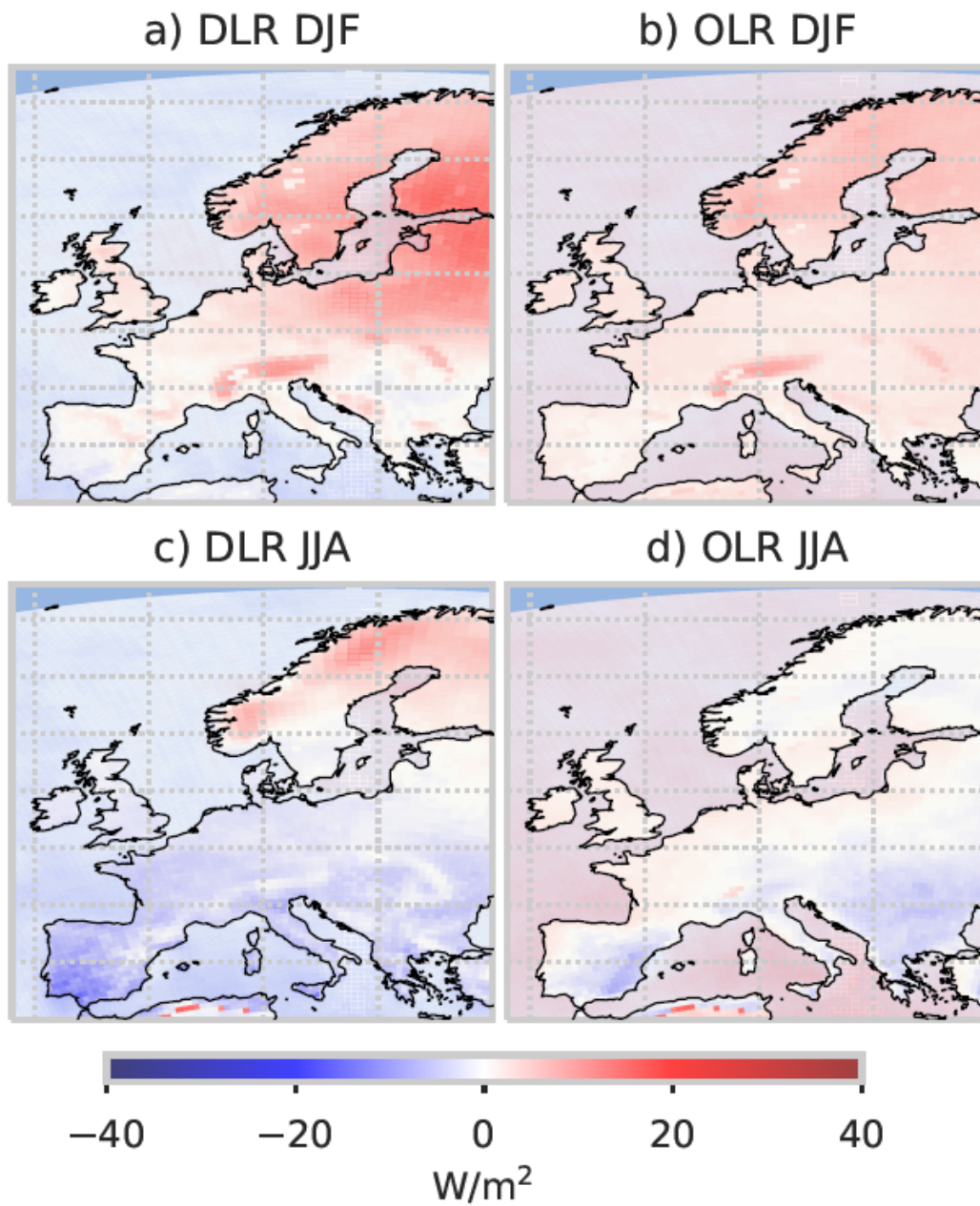
740

741

742

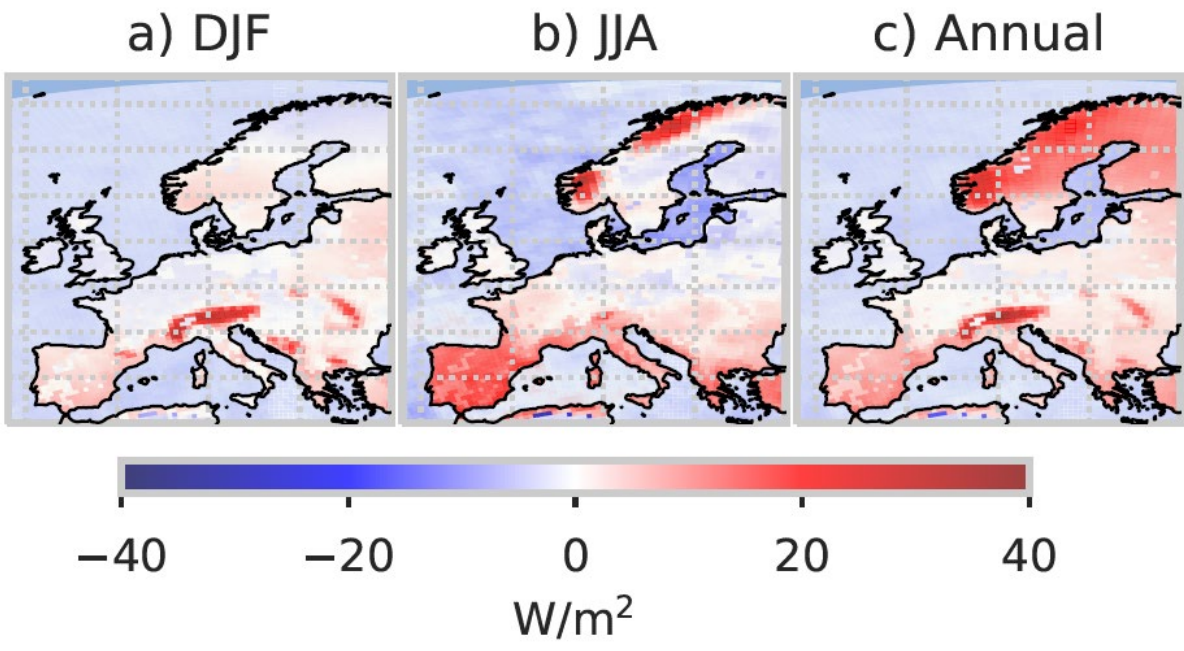
743

744



745
 746 Figure 6: Differences between CARBON and GRASS for DLR (a+c) and OLR (b+d) for the winter season
 747 (a+b) and the summer season (c+d) over the period 1986-2015.

748
 749
 750
 751
 752
 753
 754
 755
 756



757

758 Figure 7: Changes in the TOA energy balance between CARBON and GRASS for (a) winter, (b) summer
 759 and (c) the whole year.

760

761

762

763

764

765

766

767

768

769

770

771

772

773

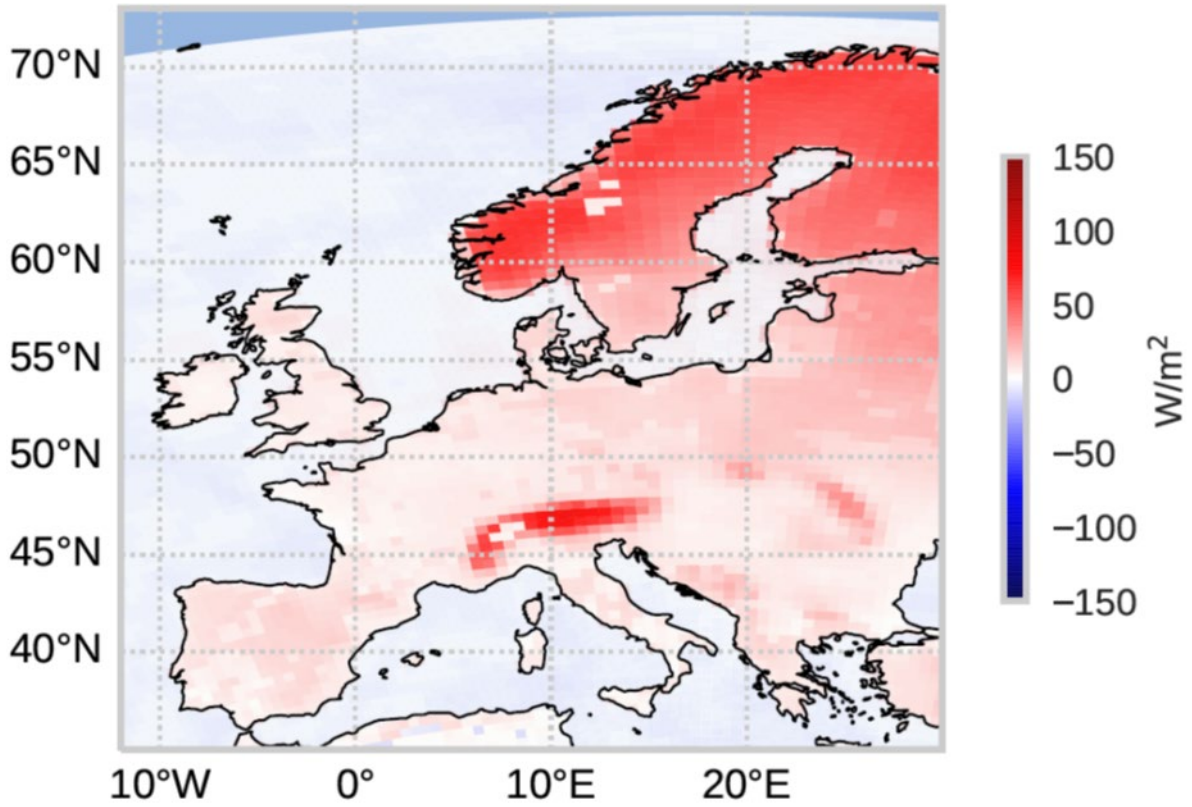
774

775

776

777

778



779

780 Figure 8: Mean differences in net shortwave radiation in spring between CARBON and GRASS for the
781 period 1986-2015.

782